Remote Sensing of Environment 132 (2013) 49–58

Contents lists available at SciVerse ScienceDirect

Remote Sensing of Environment

journal homepage: www.elsevier.com/locate/rse

Evaluating methods to detect bark beetle-caused tree mortality using single-date and multi-date Landsat imagery

Arjan J.H. Meddens [a,*], Jeffrey A. Hicke [a], Lee A. Vierling [b], Andrew T. Hudak [c]

[a] University of Idaho, Department of Geography, 810 W 7th Street, McClure Hall 203, Moscow, ID 83844-3021, USA
[b] University of Idaho, Geospatial Laboratory for Environmental Dynamics, Department of Forest, Rangeland, and Fire Sciences, Campus Box 1135, Moscow, ID, 83844-1135, USA
[c] U.S. Department of Agriculture Forest Service, Rocky Mountain Research Station, Forestry Sciences Laboratory, 1221 South Main Street, Moscow, ID 83843, USA

ARTICLE INFO

Article history:
Received 20 July 2012
Received in revised form 3 January 2013
Accepted 5 January 2013
Available online xxxx

Keywords:
Landsat
Remote sensing
Single-date
Multi-date
Time series
Bark beetles
Forest disturbance
Classification

ABSTRACT

Bark beetles cause significant tree mortality in coniferous forests across North America. Mapping beetle-caused tree mortality is therefore important for gauging impacts to forest ecosystems and assessing trends. Remote sensing offers the potential for accurate, repeatable estimates of tree mortality in outbreak areas. With the advancement of multi-temporal disturbance detection methods using Landsat data, the capability exists for improvement in mapping methods, yet more information is needed to determine the accuracy of these methods for mapping forest disturbances and to quantify differences between these methods and single-date image classification methods. We compared single-date (using maximum likelihood classification) to multi-date (using time series of spectral indices) classification methods of Landsat imagery and investigated how detection accuracy changed with varying levels of mortality severity. For each method, we evaluated several bands and/or spectral vegetation indices and identified the one that resulted in the highest accuracy. A fine-resolution classified aerial image within the Landsat scene was used as reference data for evaluation and comparison between methods. For the single-date image classification, we achieved a 91.0% (kappa = 0.88) overall accuracy with 11.7% omission and 2.3% commission errors for the red stage (tree mortality) class using the tasseled cap transformation indices of brightness, greenness, and wetness. For the multi-date analysis, the Band5/Band4 anomaly produced the highest accuracy among spectral indices and resulted in a 89.6% (kappa = 0.86) classification accuracy with 12.6% omission and 7.1% commission errors for the red stage class. We compared accuracies between the best single- and multi-date methods across a range of tree mortality within a pixel. The multi-date method was more accurate at intermediate levels of tree mortality, whereas the single-date method was more accurate at high mortality levels. Our results indicate that Landsat-based mapping of forest disturbances that use either single-date or multi-date methods can result in high classification accuracy.

© 2013 Elsevier Inc. All rights reserved.

1. Introduction

At the end of the 20th century, insects and pathogens affected >20 million ha of forests annually in the United States and resulted in annual economic losses of approximately $1.5 billion (Dale et al., 2001). Bark beetles are particularly widespread in western North America, affecting millions of ha of forest in the last few decades (Meddens et al., 2012; Raffa et al., 2008). By killing trees, bark beetles affect timber production (Schwab et al., 2009), wildfire (Hicke et al., 2012; Jenkins et al., 2008; Simard et al., 2011), forest structure and composition (Pfeifer et al., 2011; Veblen et al., 1991), wildlife habitat (Klenner & Arsenault, 2009), and esthetics and community risk perception (Flint, 2007; Flint et al., 2009).

The mountain pine beetle (*Dendroctonus ponderosae* Hopkins) is a bark beetle species that causes large forest disturbances by killing multiple species of pine, with the most important host species including lodgepole (*Pinus contorta*), ponderosa (*P. ponderosa*), and five-needle pines such as whitebark pine (*P. albicaulis*). After attack by these beetles, trees progress through a series of stages that influence spectral reflectance and therefore detectability. Mountain pine beetles attack trees in late summer, and in subsequent months the foliage of the killed trees remains visually unaltered despite reductions in foliar moisture ("green attack stage") (Wulder et al., 2006a). The trees turn red ("red stage") the year after attack. Three to five years after attack, the trees drop their needles and are in the "gray stage" (Wulder et al., 2006a).

Digital remote sensing (including satellite and aerial imagery) offers the potential for estimates of outbreak area, with high detection accuracy and repeated observations. The usefulness of remote sensing in studying insect disturbance is widely recognized (e.g., Franklin et al., 2003; Radeloff et al., 1999; Skakun et al., 2003; Wulder et al., 2006a). As trees progress from the green stage to the red stage, the chlorophyll absorption feature around 680 nm fills in (i.e., the red reflectance increases). Past studies have taken advantage of this spectral

* Corresponding author. Tel.: +1 208 885 2970; fax: +1 208 885 2855.
E-mail addresses: ameddens@uidaho.edu (A.J.H. Meddens), jhicke@uidaho.edu (J.A. Hicke), leev@uidaho.edu (L.A. Vierling), ahudak@fs.fed.us (A.T. Hudak).

0034-4257/$ – see front matter © 2013 Elsevier Inc. All rights reserved.
http://dx.doi.org/10.1016/j.rse.2013.01.002

feature by using the red-green index (RGI), the ratio of red reflectance to green reflectance (Coops et al., 2006; Hicke & Logan, 2009; Meddens et al., 2011). A number of studies to detect tree mortality from insect outbreaks have also used multispectral imagery (e.g., Kharuk et al., 2003; Radeloff et al., 1999; Skakun et al., 2003) as well as hyperspectral imagery with a large number of narrow channels (Pontius et al., 2005) to leverage the differences in the near-infrared (NIR) and shortwave infrared (SWIR) spectral regions.

Landsat imagery has often been employed for detection of insect outbreaks because of its spatial resolution, broad spatial extent, multispectral capability, and early deployment (e.g., Ahern, 1988; Franklin et al., 2003; Radeloff et al., 1999; Skakun et al., 2003). For example, high classification accuracies were achieved detecting insect disturbance with Landsat imagery using a variety of techniques that included logistic regression with ancillary data (Wulder et al., 2006b), enhanced wetness difference index (EWDI) using a threshold (Skakun et al., 2003), and maximum likelihood classification methods (Franklin et al., 2003).

Forest disturbance detection methods that use multi-date Landsat imagery over longer periods have great potential for application to characterize insect outbreaks for several reasons. First, global coverage and long periods of existence of satellite data allow multi-date analyses in many locations (Cohen & Goward, 2004). Second, the complete image archive of Landsat data has been made freely available (USGS, 2008), making multi-temporal imagery more accessible. Third, time series of classifications are useful for quantifying spatio-temporal dynamics of forest disturbance, including outbreak initiation, mortality extent and rate, and forest recovery. Two methods using multi-temporal Landsat data to detect forest disturbances have recently been described. First, Kennedy et al. (2007) developed a trajectory-based change detection method and subsequently improved upon this with the LandTrendr algorithm, which fits temporal trajectories of forest disturbance and recovery (Kennedy et al., 2010). Second, in developing a multi-temporal Landsat disturbance history classification technique called the Vegetation Change Tracker, Huang et al. (2009) calculated an “integrated forest z-score”, which is an inverse measure of the likelihood of a pixel being forested using automatically identified forest pixels and multiple Landsat bands. Both methods accurately captured the type and timing of multiple forest disturbances.

Several studies have used time series of Landsat imagery to detect insect disturbance. Time series of ratios of Landsat shortwave infrared reflectance to near-infrared reflectance were used to map forest disturbance in the southwestern US (Vogelmann et al., 2009). A normalized difference moisture index was used to classify mountain pine beetle disturbance using eight Landsat scenes over a 14-year period, resulting in overall accuracies of 71% to 86% (Goodwin et al., 2008). The LandTrendr method was recently used to characterize bark beetle and defoliator impacts on coniferous forests in Oregon and resulted in good agreement between spectral trajectories and insect-caused tree mortality (Meigs et al., 2011). In addition, they showed a statistically significant relationship between Landsat spectral change and field basal area mortality ($R^2 = 0.4$), indicating potential to use spectral deviations to estimate disturbance severity.

Several gaps exist that limit understanding of the capability of Landsat-scale resolution for detecting insect-caused tree mortality. Landsat grid cells (with a size of 0.09 ha) that exhibit trees in the red stage rarely reach 100% killed tree cover, and most grid cells exhibit intermediate levels of mortality (e.g., 20–80% canopy mortality) (Meddens et al., 2011). Therefore, more research is needed to quantify the level of mortality that can be detected by Landsat classification methods. Further, additional studies are needed to assess whether improved mapping of beetle disturbances can be achieved by following pixel trajectories through time (multi-date classification) as compared to using spectral information from a given date (single-date classification).

To address these gaps, our objectives were to investigate the efficacy of Landsat satellite imagery to quantify varying levels of tree mortality following mountain pine beetle attack. We utilized fine-resolution aerial imagery to build classifications from the coarser-resolution Landsat imagery and for evaluation. We compared the accuracy of single-date image classification with multi-date image classification (Fig. 1) and developed an evaluation technique to investigate classification accuracy across varying levels of bark beetle-caused tree mortality for both methods.

2. Methods

2.1. Study area

The study area was located in northcentral Colorado and southern Wyoming (Fig. 2a and b). The area was chosen because it is the location of a major mountain pine beetle outbreak that began in 2000 and because a previous study mapped tree mortality from fine-resolution aerial imagery in the area (Meddens et al., 2011). Mountain pine beetles have caused extensive lodgepole pine mortality in the study area. Mean average annual precipitation in the area is 51.6 cm, and average annual maximum and minimum temperatures are 9.8 and −10.2 °C, respectively (1971–2000) (Western Regional Climate Center, Frasier station, elevation: 2609 m, http://www.wrcc.dri.edu; accessed 6 April 2009). The elevation ranges from 1388 m in the plains east in the study location to almost 5000 m in the Colorado Rocky Mountains. Dominant tree species include Engelmann spruce (*Picea engelmannii*), subalpine fir (*Abies lasiocarpa*) and limber pine (*Pinus flexilis*) at higher elevations. Lodgepole pine (*P. contorta*) and occasional other tree species including aspen (*Populus tremuloides*) occur at middle elevations, approximately 2500–3100 m (Stohlgren & Bachand, 1997). Ponderosa pine (*Pinus ponderosae*) and Douglas-fir (*Pseudotsuga menziesii*) occur mostly on drier sites at lower elevations.

2.2. Landsat data preparation

Sixteen archived Landsat Thematic Mapper (TM) 5 and four Landsat Enhanced Thematic Mapper (ETM+) 7 images (Worldwide Reference System 2: Path 43/Row 34) were downloaded from the USGS GLOVIS website (http://glovis.usgs.gov; accessed: 13 September 2011) (Table 1). The chosen images were acquired close to the middle of the growing season (July/August) and with minimal cloud cover. If there was significant cloud cover in a scene, we attempted to find a second image within that same year. By visual inspection we noted that Landsat data that were terrain-corrected (processing level: L1T) resulted in high georegistration accuracy between the imagery (i.e., no noticeable image-to-image offsets were found).

Radiometric normalization was necessary for comparing reflectances across images. A base image (date: 10 August 2002) was atmospherically corrected and converted to top-of-canopy reflectance using the COST-correction method (Chavez, 1996). Subsequently, other images were radiometrically normalized to this base image following the approach of Schroeder et al. (2006), which employs the multivariate alteration detection (MAD) algorithm developed by Canty et al. (2004). The MAD algorithm uses canonical correlation analyses to find linear combinations between two images (base and target images). The sum of squares of the MAD transformation is approximately chi-square distributed and can be interpreted as no-change probabilities of a given target image. Time-invariant pixels (i.e., pixels with low chi-square values) were used to match the reflectance of the target image to the COST-corrected base image using reduced major axis regression (Cohen et al., 2003). This radiometric normalization methodology was repeated for all images in the time series.

In addition to the six shortwave TM5 and ETM+ Landsat bands (Bands 1–5, 7) (Table 2), we calculated several spectral indices to aid with image classification (Table 3). Landsat reflectances were used to calculate the red-green index (RGI), normalized difference vegetation index (NDVI), normalized difference moisture index (NDMI), and the

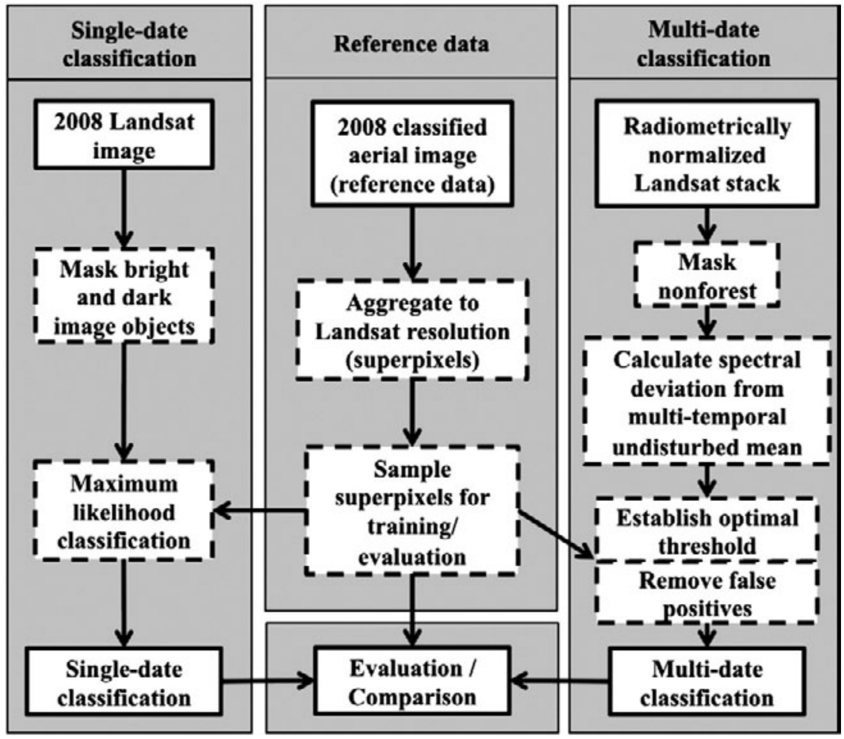

Fig. 1. Workflow of the products and operations used to classify Landsat imagery. Solid line boxes indicate products; dashed line boxes indicate operations.

Band 5/Band 4 ratio (B5/B4). Tasseled cap (TC) indices (Crist & Cicone, 1984) were computed (brightness (TCBRI), greenness (TCGRE), and wetness (TCWET)), and because we transformed the Landsat data to reflectances, we used the tasseled cap transformation for reflectance data (Crist, 1985). These seven indices were chosen because they capture most of the variation in the spectral bands and because previous research has shown that they are effective in characterizing land surfaces using satellite data (e.g., Cohen et al., 1998; Coops et al., 2006; Meddens et al., 2008; Tucker, 1979; Wilson & Sader, 2002).

2.3. Reference data

We utilized a 2008 classified aerial image of 94-km^2 that was evaluated with field data (Meddens et al., 2011). The aerial imagery contained four bands (i.e., red, green, blue, and near infrared bands) (Fig. 2c), and during classification, the 30-cm aerial image was aggregated to a 2.4-m spatial resolution to maximize classification accuracy (overall accuracy = 90%, kappa = 0.88; Meddens et al., 2011, Fig. 2d). Classes included undisturbed forest, red stage, gray stage, herbaceous

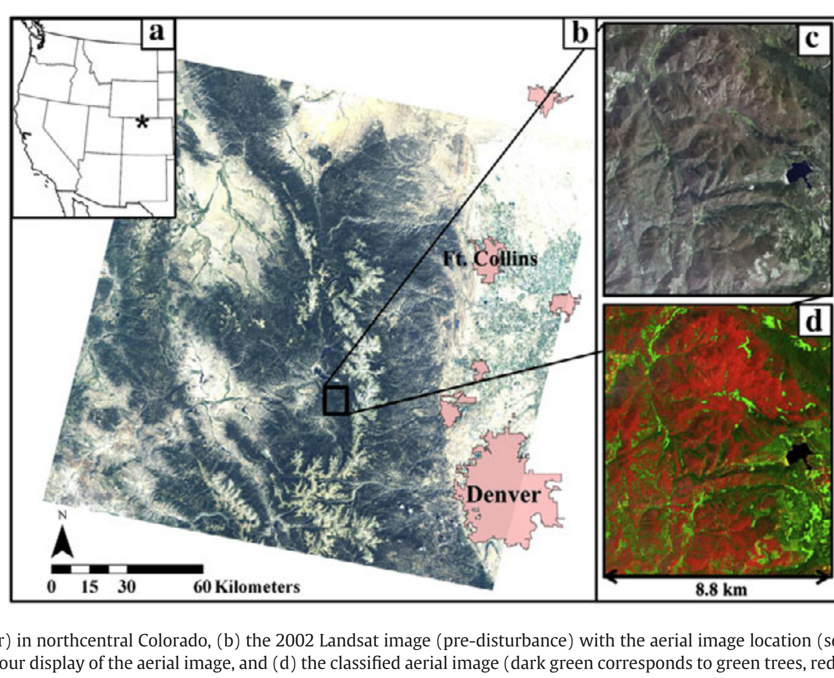

Fig. 2. (a) Study area location (star) in northcentral Colorado, (b) the 2002 Landsat image (pre-disturbance) with the aerial image location (square; used as reference data) in the centre of the image, (c) natural colour display of the aerial image, and (d) the classified aerial image (dark green corresponds to green trees, red to red stage, gray to gray stage, light green to herbaceous vegetation, yellow to bare soil, and black to shadow and water).

Table 1
Landsat imagery used in this study.

	Year	Month/day	Day of year	Sensor	Approximate cloud cover
1	1996	17 August	230	TM5	0%
2	1997	20 August	232	TM5	5%
3	1998	23 August	235	TM5	20%
4	1999[a]	2 August	214	ETM+	29%
5	1999	18 August	230	ETM+	3%
6	2000	19 July	201	TM5	5%
7	2001	22 July	203	ETM+	8%
8	2002[b]	10 August	222	ETM+	0%
9	2003	4 July	185	TM5	0%
10	2004[a]	6 July	188	TM5	6%
11	2004	7 August	220	TM5	24%
12	2005	11 September	254	TM5	0%
13	2006	28 July	209	TM5	0%
14	2007[a]	15 July	196	TM5	8%
15	2007	16 August	228	TM5	5%
16	2008[a]	2 August	215	TM5	26%
17	2008	18 August	231	TM5	9%
18	2009	21 August	233	TM5	0%
19	2010	25 September	268	TM5	0%
20	2011	27 August	239	TM5	9%

[a] Priority image for that year; second image used to fill cloudy areas in first image.
[b] Base image.

vegetation, bare soil, and shadow/water. To serve as reference data, this classification was aggregated to the 30-m Landsat pixel resolution, producing class proportions (i.e., the percentage of each class within a 30-m pixel) and modal classes (e.g., undisturbed forest, red stage). The classification captured the entire range of mountain pine beetle mortality within 30-m grid cells, from no mortality to very high mortality (Fig. 3). The classified aerial image extended the spatial coverage and the number of samples beyond what is possible with ground-based observations. We refer to the classified aerial image as *reference data*, the classified aerial image location as *reference area*, and the aggregated aerial image pixels as *superpixels* to indicate that these Landsat-size pixels consist of many smaller pixels from the aerial imagery.

In this study, we focused on immediately detectable tree mortality (i.e., the red stage) and we did not include a gray stage class. The addition of a gray stage was beyond the scope of this analysis. To overcome confounding factors of mixing multiple mortality classes, we did not sample from pixels that had >2% class proportion of the gray stage class.

Table 2
Spectral regions, spatial resolution, and temporal characteristics of Landsat TM5 and ETM+ sensors.

Sensor	TM5 launched: 1 March 1984	ETM+ launched: 15 April 1999
Spectral regions (μm)		
Band 1 (B1; blue)	0.45–0.52	0.45–0.515
Band 2 (B2; green)	0.52–0.60	0.525–0.605
Band 3 (B3; red)	0.63–0.69	0.63 – 0.69
Band 4 (B4; NIR[a])	0.76–0.90	0.75–0.90
Band 5 (B5; NIR)	1.55–1.75	1.55–1.75
Band 6 (thermal)[b]	10.40–12.50	10.40–12.50
Band 7 (B7; MIR[c])	2.08–2.35	2.09–2.35
Panchromatic band[b]	Not on sensor	0.52–0.90
Spatial resolution (m)		
Spectral bands	30	30
Thermal band[b]	120	60
Panchromatic[b]	Not on sensor	15
Temporal resolution (days)		
Repeat cycle	16	16

[a] Near infrared.
[b] Bands not used in this study.
[c] Middle infrared.

2.4. Single-date classification

We produced a single-date classification of the 2008 Landsat image (2 August 2008, matching the date of the finer-resolution aerial imagery) to compare the accuracy of single-date with that of a multi-date classification for detecting bark beetle tree mortality (Fig. 1). Classes of interest included undisturbed forest, red stage, herbaceous, and masked locations (i.e., clouds, cloud shadow, water, bare soil). By visual inspection we masked clouds and bright objects (such as soil and built-up areas) from the other image components using a threshold value of the TCBRI (TCBRI >5.3). Similarly, cloud shadow and dark image objects (such as water) were masked with values less than a given TCBRI (TCBRI <0.75).

The maximum likelihood classifier (MLHC) was applied because it is a straightforward classifier and has been used successfully in previous studies detecting tree mortality with Landsat imagery (e.g., Franklin et al., 2003). We selected nearly homogeneous superpixels from the reference data for training and evaluation as those with a class proportion of >70% for each of the undisturbed forest, red stage, herbaceous, and masked classes. We randomly sampled pixels from these selections to limit the number of pixels in any class to the minimum across all classes (herbaceous class; $n=1368$). We then randomly selected 75% of the pixels for the undisturbed forest, red stage, and herbaceous vegetation classes ($n=1026$ per class) as training data in the MLHC and used the remaining 25% for evaluation ($n=342$ per class). In addition to an evaluation with mostly homogeneous training data (>70% class proportion), we also determined classification accuracy for pixels with >50% area within one class to evaluate less homogeneous evaluation data, limiting the number of pixels in any class to the minimum across all classes (herbaceous class; $n=1930$ pixels). The 70% cutoff was chosen to select superpixels with a substantial class majority and because the 70% cutoff generated an acceptable number of samples for classification evaluation. The 50% cutoff was chosen to assess changes in results using a different threshold and because it is the lowest percentage where a given class contribution still has the majority within the superpixel.

Confusion matrices (Congalton, 1991) and kappa statistics (Cohen, 1960) were generated for several band combinations. The kappa statistic is a more conservative statistic of accuracy because the statistic corrects for image classification accuracy by chance (Cohen, 1960). We identified the best band/index combination based on high overall classification accuracy and by visual inspection of the entire Landsat scene for several iterations of the maximum likelihood classification with different band/index combinations.

2.5. Multi-date classification

For the multi-date classification, classes of interest were the same as the single-date classification. Although we screened the Landsat images for a minimum of cloud cover, some cloud cover remained in some years (Table 1). We identified clouds, cloud shadows, and dark image objects (such as water) using threshold values of TCBRI (see Table S1 for thresholds values), which varied slightly per scene. When there were clouds in the image, a second image from the same year was used to fill cloudy areas in the first image (Table 1).

After separating clouds from other image components, we separated vegetated from nonvegetated locations. We followed the notion posed in Huang et al. (2008) that forests are generally the darkest objects in a Landsat image (with the exception of cloud shadows and water) and that there exists a peak in the pixel histogram (if enough forest is present) most noticeable in Landsat bands 2, 3, and 5. We used the mode of the distribution as the threshold separating forest from nonforest. After visual inspection, we found that the green

Table 3
Landsat derived spectral indices considered in the classification (bands (B) refer to TM band order).

Index	Abbrev.	Formula	Notes	Reference
Red–green index	RGI	B3/B2	Sensitive to conifer tree mortality (especially red-stage)	Coops et al. (2006)
Normalized difference vegetation index	NDVI	(B4 − B3)/(B4 + B3)	Sensitive to green (healthy) vegetation	Tucker (1979)
Band5/Band4	B5/B4	B5/B4	Sensitive to conifer tree health	Vogelmann (1990) Vogelmann and Rock (1988) and Wilson and Sader (2002)
Normalized difference moisture index	NDMI	(B4 − B5)/(B4 + B5)	Sensitive to canopy water content	
Tasseled cap brightness	TCBRI	0.2043 ∗ B1 + 0.4158 ∗ B2 + 0.5524 ∗ B3 + 0.5741 ∗ B4 + 0.3124 ∗ B5 + 0.2303 ∗ B7	Sensitive to surface brightness	Crist (1985)
Tasseled cap greenness	TCGRE	− 0.1603 ∗ B1 − 0.2819 ∗ B2 − 0.4934 ∗ B3 + 0.7940 ∗ B4 − 0.0002 ∗ B5 − 0.1446*B7	Sensitive to vegetation greenness	
Tasseled cap wetness	TCWET	0.0315 ∗ B1 + 0.2021 ∗ B2 + 0.3102 ∗ B3 + 0.1594 ∗ B4 − 0.6806 ∗ B5–0.6109 ∗ B7	Sensitive to vegetation vigor (water content)	

band (B2) best separated vegetated and nonvegetated areas (Table S1). However, herbaceous vegetation was not well separated from the forested pixels using this method based on visual inspection. Therefore, we separated herbaceous vegetation using TCGRE from forest (disturbed and undisturbed) using a constant threshold value across all scenes (TCGRE > 1.1, Table S1).

Temporal anomalies represent the difference between a spectral index value at a given time and the multi-temporal, predisturbance mean of a given spectral index. Time series Landsat data for forested pixels preceding bark beetle disturbance were used to establish a baseline from which to distinguish spectral deviations to detect forest disturbance. The magnitude of change between the multi-temporal mean and the value at a given time was used to discriminate between disturbed and undisturbed forest pixels. We calculated temporal anomalies of spectral indices (RGI, NDVI, NDMI, B5/B4, TCBRI, TCGRE, and TCWET) in a given year from a temporal undisturbed mean for a given forested pixel. Anomalies were calculated as follows:

$$SI'_{x,y,t} = SI_{x,y,t} - \frac{\sum_{t'=1}^{n} SI_{x,y,t'}}{n} \qquad (1)$$

where SI' is the temporal anomaly of a given Landsat-derived spectral index (SI) at pixel location x, y in year t; $SI_{x,y,t}$ is the value of the spectral index for that pixel in that year; and the second term on the right-hand side of the equation is the undisturbed multi-year mean at that location for the n undisturbed years (t'). To calculate the undisturbed mean, an iterative process was employed. We first included all years in the calculation of the mean, then in subsequent iterations we removed years that were more than one standard deviation from the multi-year mean in the expected direction of disturbance (e.g., more negative for NDVI; more positive for RGI). We also removed outliers (mostly haze and cloud shadows that were not removed by the masking) deviating more than four standard deviations in the opposite direction. Iterations continued until there were no values exceeding one standard deviation in the direction of the disturbance. In addition to anomalies, we investigated a method using z-scores by dividing the anomaly by the standard deviation of the undisturbed multi-temporal mean. We found that this method did not yield more accurate results than our preferred, more straightforward anomaly approach.

Once the spectral anomalies were computed for the forested pixels, we identified years with mortality using an anomaly threshold value (Fig. 4). We removed false positives when a pixel was flagged as red stage (i.e., exceeded the threshold) in the current year but did not exceed the threshold in the subsequent year; in other words, we identified pixels as disturbed only if a given pixel exceeded the threshold for two consecutive years. Additional tests of longer periods exceeding the threshold (i.e., three years in a row) did not improve results. Using the evaluation data set described above in the single-date classification section (>70% class proportions), we generated confusion matrices (Congalton, 1991) for different anomaly threshold values for each spectral anomaly. For each spectral index anomaly, we identified the highest overall accuracy across this range of thresholds for separating undisturbed forest from insect-disturbed red stage forest locations. Similar to the single-date classification, we also calculated confusion matrices for >50% class proportions for the different anomalies.

2.6. Comparison of classification methods

We evaluated the classification accuracy between single- and multi-date classifications for different amounts of tree mortality within a

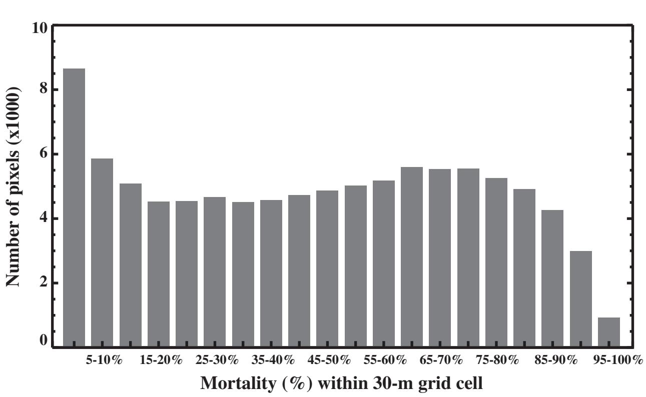

Fig. 3. Frequency distribution of mountain pine beetle-caused tree mortality (percentages) within 30-m resolution pixels (area = 0.09 ha) generated from classified and aggregated aerial imagery used as reference data.

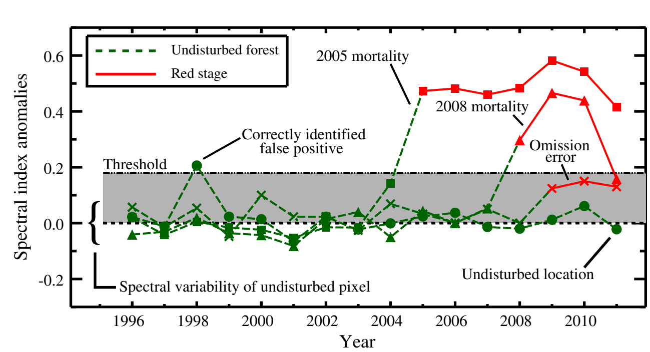

Fig. 4. Examples of temporal pixel trajectories representing anomalies from an undisturbed mean of Landsat time series data. The threshold indicated in the figure was used for discriminating between disturbed and undisturbed forest pixels in the multi-year Landsat image classification (i.e., above or below the threshold, respectively).

Table 4
Overall accuracy and kappa values (in parentheses) for different spectral index combinations used in the single-date maximum likelihood classification. Confusion matrices were computed with reference data (aerial imagery) with >50% and >70% class proportions. The classification using the TCBRI, TCGRE, and TCWET was used in further analyses.

Spectral band and index combinations	Reference data with >50% class proportion	Reference data with >70% class proportion
TCBRI, TCGRE, TCWET	84.8% (0.80)	91.0% (0.88)
RGI, NDVI, B4	85.3% (0.80)	90.8% (0.88)
B2, RGI	79.4% (0.72)	84.5% (0.79)
B2, B5, NDVI	85.5% (0.81)	90.4% (0.87)

Landsat pixel. From the reference data, we selected superpixels of >90% undisturbed forest and superpixels for increasing red stage class proportion (0–10%, 10–20%, 20–30%, 30–40%, 40–50%, 50–60%, 60–70%, 70–80%, 80–90%, 90–100%). Because there were only a limited number of pixels in the high mortality classes (<100 pixels), we randomly selected 50–pixel locations for each of these bins and repeated this selection ten times (with replacement), computing classification accuracy metrics for each selection. All processing and analyses in this study were performed using the Interactive Data Language (IDL, version 7.0.1, Exelis Visual Information Solutions; http://www.exelisvis.com, accessed 17 October 2012).

3. Results

3.1. Single-date classification

The maximum likelihood classification with the three tasseled cap indices (TCBRI, TCGRE, TCWET) resulted in the single-date classification with highest classification accuracy (Table 4). The overall classification accuracy for the maximum likelihood classification of the single-date 2008 Landsat image was 91.0% (kappa = 0.88) with high accuracies for all classes (Table 5). The red stage class omission error for the single-date classification was 11.7% and the commission error was 2.3%. We found other band/index combinations (e.g., RGI, NDVI, B4) that resulted in comparable accuracies, however, after visual inspection, we determined that these resulted in substantial number of commission errors (false positives) in areas outside of the reference area. When we evaluated the classification with less homogeneous pixels than the >70% class proportions (i.e., superpixels with >50% class proportions), the classification accuracy using the TCBRI, TCGRE, and TCWET band combination decreased to 84.8% (kappa = 0.80) (Table 6).

3.2. Multi-date classification

The B5/B4 spectral anomaly (B5/B4′) resulted in the highest classification performance among all the spectral anomalies analyzed (RGI′, NDVI′, NDMI′, TCWET′, TCBRI′, TCGRE′, and B5/B4′) (Table 7). The threshold value of the B5/B4′ maximizing classification accuracy was 0.18 (Fig. 5). Values above this threshold correctly identified fewer red stage pixels (more conservative), resulting in decreased accuracy because of increases in omission error. For values below this threshold, the accuracy of the undisturbed forest class decreased because of commission errors in the red stage class (false positives).

Using the 0.18 threshold value for B5/B4′, the overall classification accuracy for the 2008 Landsat classification was 89.4% (kappa = 0.86) with high accuracies across all classes (Table 8). The red stage class omission error for the multi-date classification was 12.6% and the commission error was 7.1%. The greatest confusion existed between undisturbed forest and red stage classes and between the red stage and masked classes. When we performed evaluation of reference data with more mixed pixels (i.e., superpixels with >50% of any class), the classification accuracy decreased to 83.2% (kappa = 0.78) (Table 9).

3.3. Comparison of classification methods

Red stage class accuracy rapidly decreased with decreasing amounts of tree mortality (red stage) within a Landsat pixel for both single- and multi-date classification methods (Fig. 6). Classification accuracy of pixels with >60% red stage was above 75%, and classification accuracy of pixels with <40% red stage was less than 50%. The single-date classification resulted on average in 8% higher red stage class accuracy than the multi-date classification for the highest levels of red stage (i.e., >70%). The multi-date classification however, resulted in 12% higher red stage class accuracy on average than the single-date classification, for intermediate levels (20–70%). Differences in accuracy between single and multi-date approaches were mainly a result of omission errors (i.e. false negatives) rather than commission errors (Fig. 6b and c).

4. Discussion

We found that the classification that used the tasseled cap indices (brightness, greenness, wetness) produced the highest accuracy for the single-date approach. Among seven indices evaluated for the multi-date approach, the B5/B4 anomalies resulted in the most accurate classification. We found high classification accuracies for mapping beetle-caused tree mortality using both single- and multi-date methods. Overall accuracies with respect to the collocated aerial imagery classification were comparable between single- and multi-date classification methods (91% versus 90%, respectively), indicating that multi-date methods (by following pixel trajectories through time) did not improve overall classification accuracy.

A wide range mortality severity of values occurred within the 30-m superpixels (Fig. 3). High classification accuracies were obtained for high levels of tree mortality within pixels, whereas for pixels exhibiting

Table 5
Confusion matrix of the 2008 single-date image classification using the maximum likelihood classifier with TCBRI, TCGRE, and TCWET indices and pixel locations from aggregated classified aerial imagery with >70% class proportions (numbers of pixels and in parentheses percentages).

		Reference data from aerial image						
	Class	Undisturbed forest	Red stage	Herb.	Mask	Total	Comm. error	User acc.
Classification	Undisturbed forest	**307 (89.8%)**	10 (2.9%)	8 (2.3%)	3 (0.9%)	328	6.4%	93.6%
	Red stage	6 (1.8%)	**302 (88.3%)**	0 (0.0%)	1 (0.3%)	309	2.3%	97.7%
	Herbaceous	11 (3.2%)	0 (0.0%)	**298 (87.1%)**	0 (0.0%)	309	3.6%	96.4%
	Mask	18 (5.3%)	30 (8.8%)	36 (10.5%)	**338 (98.8%)**	422	19.9%	80.1%
	Total (pixels)	342	342	342	342	1368		
	Omis. error	10.2%	11.7%	12.9%	1.2%	Overall Acc. = 91.0%		
	Prod. acc.	89.8%	88.3%	87.1%	98.8%	Kappa = 0.88		

Significance of bold Emphasizes the individual class accuracies of the different classes.

Table 6
Confusion matrix of the 2008 single-date image classification using the maximum likelihood classifier with TCBRI, TCGRE, and TCWET indices and pixel locations from aggregated classified aerial imagery with >50% class proportions (numbers of pixels and in parenthesis percentages).

		Reference data from aerial image						
	Class	Undisturbed forest	Red stage	Herb.	Mask	Total	Comm. error	User acc.
Classification	Undisturbed forest	**1539 (79.7%)**	183 (9.5%)	137 (7.1%)	37 (1.9%)	1896	18.8%	81.2%
	Red stage	175 (9.1%)	**1610 (83.4%)**	0 (0.0%)	4 (0.2%)	1789	10.0%	90.0%
	Herbaceous	104 (5.4%)	8 (0.4%)	**1520 (78.8%)**	8 (0.4%)	1640	7.3%	92.7%
	Mask	112 (5.8%)	129 (6.7%)	273 (14.1%)	**1881 (97.5%)**	2395	21.5%	78.5%
	Total (pixels)	1930	1930	1930	1930	7720		
	Omis. error	20.3%	16.6%	21.2%	2.5%	Overall Acc. = 84.8%		
	Prod. acc.	79.7%	83.4%	78.8%	97.5%	Kappa = 0.80		

Significance of bold Emphasizes the individual class accuracies of the different classes.

less mortality, we achieved lower detection accuracies for both the multi-date and single-date classifications. This reduction in accuracy was expected because detection using spectra from more homogeneous pixels typically results in better separability between map categories (e.g., Mayaux et al., 2006; Meddens et al., 2011). Omission errors were most prevalent for pixels exhibiting low levels of red stage class (Fig. 6). This result is similar to that of Negron-Juarez et al. (2011), who reported underestimation of subpixel-level tree mortality detection (small forest gaps) in the Amazon using Landsat data. At higher levels of tree mortality, the accuracy of the single-date classification was greater. Conversely, at lower levels of tree mortality, the multi-date classification detected mortality with higher accuracy. The possibility of detecting lower amounts of tree mortality at 30-m spatial resolution (which is more prevalent in the study area (Fig. 3), and likely across the broader region) with higher accuracy by following a pixel through time is an advantage over single-date classification methods.

Our findings indicate the usefulness of Landsat for detecting severe insect disturbance (i.e., killing >~25% of trees in the canopy within a pixel), whereas finer spatial resolution data might be necessary to detect dispersed tree mortality (i.e., single trees) across the forested landscapes (Meddens et al., 2011). Our method cannot detect slowly progressing disturbances within a pixel, such as outbreaks that result in fewer than 25% red trees cumulatively at any one time, with high accuracy.

Our cumulative red stage tree mortality estimates derived from the multi-date Landsat classification (34% of the total forest area) were within the lower and more realistic upper estimates of cumulative mortality area from aerial surveys (Meddens et al., 2012) (4 and 58%, respectively). The correlation coefficient between tree mortality area computed from the multi-date Landsat classification and the annual (new) tree mortality from the aerial surveys (upper estimate) was 0.76. Several reasons likely caused differences between the Landsat and aerial survey results. First, the aerial surveys are conducted by trained observers flying in aircraft, are subjective measures that are not repeatable, and as such are likely more uncertain. Second, clouds and cloud shadows reduced mortality area from the Landsat imagery. Finally, in some locations we noticed a difference of one year in the Landsat-based detection of the red stage compared with the visual detection of new mortality from the aerial surveyors. Additional research is required to determine the cause of this difference, but may indicate an advantage of methods using the visible part of the spectrum (including aerial surveys) for earlier detection. Thomas et al. (2011) used the Vegetation Change Tracker algorithm to map disturbance with Landsat data. Similar to our findings, these authors found that accuracy of disturbance detection increased when considering a range of detection years that included 1–2 years before to 1–2 years after the actual year of disturbance.

Our methods utilized a classified high-resolution aerial image (reference data) to aid in the methods development such as determining thresholds. This reference image effectively served to bridge the scaling gap between individual tree mortality measures and the 30-m resolution of Landsat imagery. The method improves upon those using field observations of individual trees or small plots, which can be limited in number, resulting in fewer samples, and rarely cover an entire 30-m

Table 7
Overall accuracy and kappa values (in parentheses) for different spectral anomalies used in the Landsat multi-date classification evaluated for 2008 (the year of the reference data). Confusion matrices were computed with reference data (aerial imagery) with >50% and >70% class proportions and the optimal threshold for each of the spectral anomalies. The classification using the B5/B4′ was used in further analyses.

Spectral anomaly	Reference data with >50% class proportion	Reference data with >70% class proportion
B5/B4′	83.2% (0.78)	89.6% (0.86)
RGI′	78.0% (0.71)	83.5% (0.78)
NDVI′	76.8% (0.69)	79.9% (0.73)
NDMI′	75.8% (0.68)	80.6% (0.74)
TCBRI′	75.9% (0.68)	82.7% (0.77)
TCWET′	74.5% (0.66)	77.0% (0.69)
TCGRE′	71.0% (0.61)	75.0% (0.67)

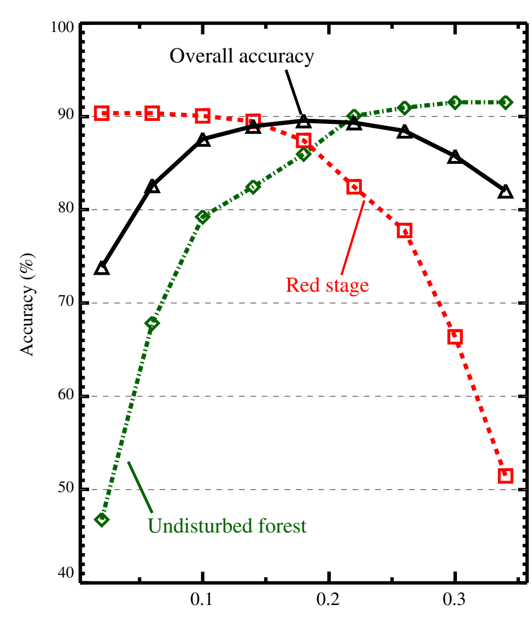

Fig. 5. Overall accuracy (black line), undisturbed forest class accuracy (green line), and red stage class accuracy (red line) from confusion matrices with different B5/B4′ threshold values used to separate undisturbed from insect-disturbed pixel locations (multi-date classification). (For interpretation of the references to colour in this figure legend, the reader is referred to the web version of this article.)

Table 8
Confusion matrix of the Landsat 2008 multi-date image classification using the optimized Band5/Band4 anomaly (B5/B4′) threshold (=0.18) and pixel locations from aggregated classified aerial imagery with >70% class proportions (numbers of pixels and in parentheses percentages).

		Reference data from aerial image						
	Class	Undisturbed forest	Red stage	Herb.	Mask	Total	Comm. error	User acc.
Classification	Undisturbed forest	**294** **(86.0%)**	16 (4.7%)	8 (2.3%)	5 (1.5%)	323	9.0%	91.0%
	Red stage	20 (5.8%)	**299** **(87.4%)**	2 (0.6%)	1 (0.3%)	322	7.1%	92.9%
	Herbaceous	11 (3.2%)	0 (0.0%)	**296** **(86.5%)**	0 (0.0%)	307	3.6%	96.4%
	Mask	17 (5.0%)	27 (7.9%)	36 (10.5%)	**336** **(98.2%)**	416	19.2%	80.8%
	Total (pixels)	342	342	342	342	1368		
	Omis. error	14.0%	12.6%	13.5%	1.8%	Overall Acc. = 89.6%		
	Prod. acc.	86.0%	87.4%	86.5%	98.2%	Kappa = 0.86		

Significance of bold Emphasizes the individual class accuracies of the different classes.

pixel. Our reference data provided complete spatial coverage within a 94-km^2 area at a 30-m resolution. Similar to the usage of the classified aerial image to bridge the scaling gap between individual tree mortality and the 30-m resolution of Landsat imagery, the classified multi-temporal Landsat imagery in this study can be used to bridge the scaling gap between medium-resolution measurements (with regional extent; i.e., Landsat) and coarser-resolution (e.g., MODIS data). Therefore, the methods and data set developed in this study will be instrumental to assess the ability of forest insect disturbance detection using MODIS products.

Although usage of high-resolution imagery for insect tree mortality detection is becoming more common (e.g., Coops et al., 2006; Hicke & Logan, 2009; Meddens et al., 2011; White et al., 2005; Wulder et al., 2008), often this detailed information is not available for method development and evaluation using coarser-resolution imagery, complicating the application of our method to other Landsat scenes. One approach that may be useful is the onscreen selection of pixels that exhibit no disturbance (within forests) and pixels exhibiting high levels of tree mortality (close to 100%) and subsequent single-date image classification using these locations. Such methods using fine-resolution (2.4 m) imagery have compared well to results developed from ground-based observations (e.g., Hicke & Logan, 2009) but have yet to be assessed with Landsat-scale resolutions. Onscreen selection of pixels may improve the extent of evaluation to the entire scene. The methods in this study were only evaluated for the reference area, and we applied our approach outside that area without an evaluation of this extrapolation.

According to USFS aerial surveys, the predominant disturbance within the Landsat scene was mountain pine beetle tree mortality occurring mainly within lodgepole pine-dominated forests. However, other types of disturbances did exist within the Landsat scene and study period. Our insect disturbance detection methodology did not attempt to separate disturbance from different insects nor separate disturbance within different host types. Determined by visual inspection, clear-cuts and other large disturbances (e.g., fires) resulting in bright pixel reflectances were automatically masked by the threshold method and were thus correctly separated from insect disturbance. Partial disturbances, such as thinning, and pixel locations not resulting in high reflective values after disturbance, such as immediately following fire (resulting in dark soil), were sometimes misclassified as insect disturbance as determined by visual inspection. Meigs et al. (2011) separated rapid insect disturbance (more often caused by bark beetles) from gradual disturbance (more often caused by defoliators) using different spectral trajectories in Oregon. More research is needed to improve automated attribution of different types of disturbances (such as forest harvest (clear-cut), thinning, bark beetle, defoliator, drought, windthrow) within a single Landsat scene across years.

Our analysis built upon earlier research using Landsat imagery to detect insect disturbance. The maximum likelihood classification for detection tree mortality with Landsat single-date imagery has been widely recognized (e.g., Franklin et al., 2003) and proved yet again successful. Our newly developed method that tracks Landsat pixels through time resembles methods from Kennedy et al. (2007) and Kennedy et al. (2010). However, our method uses deviations from an undisturbed multi-year mean to detect insect disturbance, whereas their methods include fitting idealized pixel trajectories (Kennedy et al., 2007) or fitting temporal trajectories via a segmentation process (Kennedy et al., 2010) requiring various additional computing steps. Previous research showed that Landsat B5/B4 was effective for remote mapping of conifer damage in the northeastern US (Vogelmann, 1990; Vogelmann & Rock, 1988) and assessing gradual forest changes likely associated with defoliator impacts in the southwestern US (Vogelmann et al., 2009). Our analyses did not make use of automated cloud and cloud shadow masking (e.g., Zhu & Woodcock, 2012), which assists broader applications such as automated time series Landsat classification. Future research will focus on separating

Table 9
Confusion matrix of the Landsat 2008 multi-date image classification using the optimized Band5/Band4 anomaly (B5/B4′) threshold (=0.18) and pixel locations from aggregated classified aerial imagery with >50% class proportions (numbers of pixels and in parentheses percentages).

		Reference data from aerial image						
	Class	Undisturbed forest	Red stage	Herb.	Mask	Total	Comm. error	User acc.
Classification	Undisturbed forest	**1437** **(74.5%)**	179 (9.3%)	122 (6.3%)	52 (2.7%)	1790	19.7%	80.3%
	Red stage	318 (16.5%)	**1642** **(85.1%)**	50 (2.6%)	9 (0.5%)	2019	18.7%	81.3%
	Herbaceous	73 (3.8%)	1 (0.1%)	**1479** **(76.6%)**	3 (0.2%)	1556	4.9%	95.1%
	Mask	102 (5.3%)	108 (5.6%)	279 (14.5%)	**1866** **(96.7%)**	2355	20.8%	79.2%
	Total (pixels)	1930	1930	1930	1930	7720		
	Omis. error	25.5%	14.9%	23.4%	3.3%	Overall Acc. = 83.2%		
	Prod. acc.	74.5%	85.1%	76.6%	96.7%	Kappa = 0.78		

Significance of bold Emphasizes the individual class accuracies of the different classes.

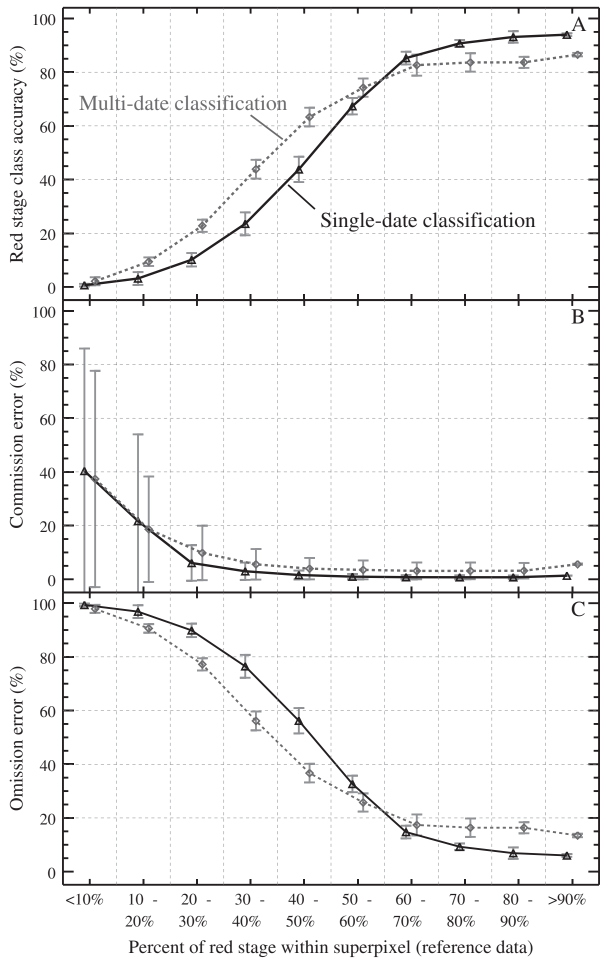

Fig. 6. (a) Red stage class accuracy, (b) red stage commission error, and (c) red stage omission error for single- (solid line) and multi-date (broken line) classifications. Accuracy and error rates were calculated from ten times recalculated confusion matrices selecting different random sets of evaluation pixels. Reference data taken from classified aerial imagery (i.e., percent red stage within superpixels). Error bars indicate the standard deviation.

the red from the gray stage, assess forest recovery following different disturbances, and attribute causes to different disturbance types using multi-date Landsat data.

5. Conclusions

Our study demonstrates the usefulness of fine-resolution aerial imagery as a reference data set for classification development and evaluation of Landsat imagery. By using the fine-resolution classification (itself having high classification accuracy; Meddens et al., 2011) as reference data, we could extend the spatial coverage and number of samples far beyond what was practical with ground-based observations. We found similar and high overall classification accuracy using both single- and multi-date image methods for mapping bark beetle-caused tree mortality, although the multi-date method produced higher accuracies at lower levels of mortality.

Tree mortality caused by biotic disturbances, warming/drought, and their interactions has been increasing in recent years (Allen et al. 2010; Meddens et al., 2012; Raffa et al., 2008). Our methods inform efforts to map tree mortality for larger regions, such as those using MODIS. Our data set of classified Landsat time series mapping bark beetle-caused tree mortality will be useful for evaluating those larger-scale studies. In addition, the data set will inform studies that increase understanding about tree mortality, including documenting spatial and temporal patterns, understanding drivers, and assessing impacts on forest fuels, hydrology, and biogeochemical cycles (e.g., the carbon cycle).

Supplementary data to this article can be found online at http://dx.doi.org/10.1016/j.rse.2013.01.002.

Acknowledgements

This research was supported by NOAA grant NA09OAR4310194, NSF ETBC grant 0910831, Los Alamos National Laboratory, USDA Forest Service Western Wildland Environmental Threat Assessment Center, and a cooperative agreement with the USGS LANDFIRE project. We gratefully acknowledge helpful comments from three anonymous reviewers and thank the following people for discussions on research directions and algorithm development: James Vogelmann, Ben Bright, Jan Eitel, Steven Garrity, and Robert Kennedy.

References

Ahern, F. J. (1988). The effects of bark beetle stress on the foliar spectral reflectance of lodgepole pine. *International Journal of Remote Sensing*, *9*, 1451–1468.
Allen, C. D., Macalady, A. K., Chenchouni, H., Bachelet, D., McDowell, N., Vennetier, M., Kitzberger, T., Rigling, A., Breshears, D. D., Hogg, E. H., Gonzalez, P., Fensham, R., Zhang, Z., Castro, J., Demidova, N., Lim, J. -H., Allard, G., Running, S. W., Semerci, A., & Cobb, N. (2010). A global overview of drought and heat-induced tree mortality reveals emerging climate change risks for forests. *Forest Ecology and Management*, *259*, 660–684.
Canty, M. J., Nielsen, A. A., & Schmidt, M. (2004). Automatic radiometric normalization of multitemporal satellite imagery. *Remote Sensing of Environment*, *91*, 441–451.
Chavez, P. S. (1996). Image-based atmospheric corrections revisited and improved. *Photogrammetric Engineering and Remote Sensing*, *62*, 1025–1036.
Cohen, J. (1960). A coefficient of agreement for nominal scales. *Educational and Psychological Measurement*, *20*, 37–46.
Cohen, W. B., Fiorella, M., Gray, J., Helmer, E., & Anderson, K. (1998). An efficient and accurate method for mapping forest clearcuts in the Pacific Northwest using Landsat imagery. *Photogrammetric Engineering and Remote Sensing*, *64*, 293–300.
Cohen, W. B., & Goward, S. N. (2004). Landsat's role in ecological applications of remote sensing. *Bioscience*, *54*, 535–545.
Cohen, W. B., Maiersperger, T. K., Gower, S. T., & Turner, D. P. (2003). An improved strategy for regression of biophysical variables and Landsat ETM+ data. *Remote Sensing of Environment*, *84*, 561–571.
Congalton, R. (1991). A review of assessing the accuracy of classifications of remotely sensed data. *Remote Sensing of Environment*, *37*, 35–46.
Coops, N. C., Johnson, M., Wulder, M. A., & White, J. C. (2006). Assessment of QuickBird high spatial resolution imagery to detect red attack damage due to mountain pine beetle infestation. *Remote Sensing of Environment*, *103*, 67–80.
Crist, E. P. (1985). A TM tasseled cap equivalent transformation for reflectance factor data. *Remote Sensing of Environment*, *17*, 301–306.
Crist, E. P., & Cicone, R. C. (1984). A physically-based transformation of Thematic Mapper data — The TM tasseled cap. *IEEE Transactions on Geoscience and Remote Sensing*, *22*, 256–263.
Dale, V. H., Joyce, L. A., McNulty, S., Neilson, R. P., Ayres, M. P., Flannigan, M. D., et al. (2001). Climate change and forest disturbances. *Bioscience*, *51*, 723–734.
Flint, C. G. (2007). Changing forest disturbance regimes and risk perceptions in Homer, Alaska. *Risk Analysis*, *27*, 1597–1608.
Flint, C. G., McFarlane, B., & Muller, M. (2009). Human dimensions of forest disturbance by insects: An international synthesis. *Environmental Management*, *43*, 1174–1186.
Franklin, S. E., Wulder, M. A., Skakun, R. S., & Carroll, A. L. (2003). Mountain pine beetle red-attack forest damage classification using stratified Landsat TM data in British Columbia, Canada. *Photogrammetric Engineering and Remote Sensing*, *69*, 283–288.
Goodwin, N. R., Coops, N. C., Wulder, M. A., Gillanders, S., Schroeder, T. A., & Nelson, T. (2008). Estimation of insect infestation dynamics using a temporal sequence of Landsat data. *Remote Sensing of Environment*, *112*, 3680–3689.
Hicke, J. A., Johnson, M. C., Hayes, J. L., & Preisler, H. K. (2012). Effects of bark beetle-caused tree mortality on wildfire. *Forest Ecology and Management*, *271*, 81–90.
Hicke, J. A., & Logan, J. A. (2009). Mapping whitebark pine mortality caused by a mountain pine beetle outbreak with high spatial resolution satellite imagery. *International Journal of Remote Sensing*, *30*, 4427–4441.
Huang, C. Q., Coward, S. N., Masek, J. G., Thomas, N., Zhu, Z. L., & Vogelmann, J. E. (2009). An automated approach for reconstructing recent forest disturbance history using dense Landsat time series stacks. *Remote Sensing of Environment*, *114*, 183–198.
Huang, C. Q., Song, K., Kim, S., Townshend, J. R. G., Davis, P., Masek, J. G., et al. (2008). Use of a dark object concept and support vector machines to automate forest cover change analysis. *Remote Sensing of Environment*, *112*, 970–985.
Jenkins, M. J., Hebertson, E., Page, W., & Jorgensen, C. A. (2008). Bark beetles, fuels, fires and implications for forest management in the Intermountain West. *Forest Ecology and Management*, *254*, 16–34.
Kennedy, R. E., Cohen, W. B., & Schroeder, T. A. (2007). Trajectory-based change detection for automated characterization of forest disturbance dynamics. *Remote Sensing of Environment*, *110*, 370–386.

Kennedy, R. E., Yang, Z., & Cohen, W. B. (2010). Detecting trends in forest disturbance and recovery using yearly Landsat time series: 1. LandTrendr — Temporal segmentation algorithms. *Remote Sensing of Environment*, *114*, 2897–2910.

Kharuk, V. I., Ranson, K. J., Kuz'michev, V. V., & Im, S. (2003). Landsat-based analysis of insect outbreaks in southern Siberia. *Canadian Journal of Remote Sensing*, *29*, 286–297.

Klenner, W., & Arsenault, A. (2009). Ponderosa pine mortality during a severe bark beetle (Coleoptera: Curculionidae, Scolytinae) outbreak in southern British Columbia and implications for wildlife habitat management. *Forest Ecology and Management*, *258*, S5–S14.

Mayaux, P., Eva, H., Gallego, J., Strahler, A. H., Herold, M., Agrawal, S., et al. (2006). Validation of the global land cover 2000 map. *IEEE Transactions on Geoscience and Remote Sensing*, *44*, 1728–1739.

Meddens, A. J. H., Hicke, J. A., & Ferguson, C. A. (2012). Spatiotemporal patterns of observed bark beetle-caused tree mortality in British Columbia and the western United States. *Ecological Applications*, *22*, 1876–1891.

Meddens, A. J. H., Hicke, J. A., & Vierling, L. A. (2011). Evaluating the potential of multispectral imagery to map multiple stages of tree mortality. *Remote Sensing of Environment*, *115*, 1632–1642.

Meddens, A. J. H., Hudak, A. T., Evans, J. S., Gould, W. A., & Gonzalez, G. (2008). Characterizing forest fragments in boreal, temperate, and tropical ecosystems. *Ambio*, *37*, 569–576.

Meigs, G. W., Kennedy, R. E., & Cohen, W. B. (2011). A Landsat time series approach to characterize bark beetle and defoliator impacts on tree mortality and surface fuels in conifer forests. *Remote Sensing of Environment*, *115*, 3707–3718.

Negron-Juarez, R. I., Chambers, J. Q., Marra, D. M., Ribeiro, G. H. P. M., Rifai, S. W., Higuchi, N., et al. (2011). Detection of subpixel treefall gaps with Landsat imagery in Central Amazon forests. *Remote Sensing of Environment*, *115*, 3322–3328.

Pfeifer, E. M., Hicke, J. A., & Meddens, A. J. H. (2011). Observations and modeling of aboveground tree carbon stocks and fluxes following a bark beetle outbreak in the western United States. *Global Change Biology*, *17*, 339–350.

Pontius, J., Hallett, R., & Martin, M. (2005). Using AVIRIS to assess hemlock abundance and early decline in the Catskills, New York. *Remote Sensing of Environment*, *97*, 163–173.

Radeloff, V. C., Mladenoff, D. J., & Boyce, M. S. (1999). Detecting jack pine budworm defoliation using spectral mixture analysis: Separating effects from determinants. *Remote Sensing of Environment*, *69*, 156–169.

Raffa, K. F., Aukema, B. H., Bentz, B. J., Carroll, A. L., Hicke, J. A., Turner, M. G., et al. (2008). Cross-scale drivers of natural disturbances prone to anthropogenic amplification: The dynamics of bark beetle outbreaks. *Bioscience*, *58*, 501–517.

Schroeder, T. A., Cohen, W. B., Song, C. H., Canty, M. J., & Yang, Z. Q. (2006). Radiometric correction of multi-temporal Landsat data for characterization of early successional forest patterns in western Oregon. *Remote Sensing of Environment*, *103*, 16–26.

Schwab, O., Maness, T., Bull, G., & Roberts, D. (2009). Modeling the effect of changing market conditions on mountain pine beetle salvage harvesting and structural changes in the British Columbia forest products industry. *Canadian Journal of Forest Research*, *39*, 1806–1820.

Simard, M., Romme, W. H., Griffin, J. M., & Turner, M. G. (2011). Do mountain pine beetle outbreaks change the probability of active crown fire in lodgepole pine forests? *Ecological Monographs*, *81*, 3–24.

Skakun, R. S., Wulder, M. A., & Franklin, S. E. (2003). Sensitivity of the thematic mapper enhanced wetness difference index to detect mountain pine beetle red-attack damage. *Remote Sensing of Environment*, *86*, 433–443.

Stohlgren, T. J., & Bachand, R. R. (1997). Lodgepole pine (*Pinus contorta*) ecotones in Rocky Mountain National Park, Colorado, USA. *Ecology*, *78*, 632–641.

Thomas, N. E., Huang, C., Goward, S. N., Powell, S., Schleeweis, K., & Hinds, A. (2011). Validation of North American Forest Disturbance dynamics derived from Landsat time series stacks. *Remote Sensing of Environment*, *115*, 19–32.

Tucker, C. J. (1979). Red and photographic infrared linear combinations for monitoring vegetation. *Remote Sensing of Environment*, *8*, 127–150.

USGS (2008). Imagery for Everyone. Timeline Set to Release Entire USGS Landsat Archive at No Charge. http://landsat.usgs.gov/documents/USGS_Landsat_Imagery_Release.pdf

Veblen, T. T., Hadley, K. S., Reid, M. S., & Rebertus, A. J. (1991). The response of sub-alpine forests to spruce beetle outbreak in Colorado. *Ecology*, *72*, 213–231.

Vogelmann, J. E. (1990). Comparison between 2 vegetation indexes for measuring different types of forest damage in the north-eastern United States. *International Journal of Remote Sensing*, *11*, 2281–2297.

Vogelmann, J. E., & Rock, B. N. (1988). Assessing forest damage in high-elevation coniferous forests in Vermont and New-Hampshire using Thematic Mapper data. *Remote Sensing of Environment*, *24*, 227–246.

Vogelmann, J. E., Tolk, B., & Zhu, Z. L. (2009). Monitoring forest changes in the southwestern United States using multitemporal Landsat data. *Remote Sensing of Environment*, *113*, 1739–1748.

White, J. C., Wulder, M. A., Brooks, D., Reich, R., & Wheate, R. D. (2005). Detection of red attack stage mountain pine beetle infestation with high spatial resolution satellite imagery. *Remote Sensing of Environment*, *96*, 340–351.

Wilson, E. H., & Sader, S. A. (2002). Detection of forest harvest type using multiple dates of Landsat TM imagery. *Remote Sensing of Environment*, *80*, 385–396.

Wulder, M. A., Dymond, C. C., White, J. C., Leckie, D. G., & Carroll, A. L. (2006a). Surveying mountain pine beetle damage of forests: A review of remote sensing opportunities. *Forest Ecology and Management*, *221*, 27–41.

Wulder, M. A., White, J. C., Bentz, B., Alvarez, M. F., & Coops, N. C. (2006b). Estimating the probability of mountain pine beetle red-attack damage. *Remote Sensing of Environment*, *101*, 150–166.

Wulder, M. A., White, J. C., Coops, N. C., & Butson, C. R. (2008). Multi-temporal analysis of high spatial resolution imagery for disturbance monitoring. *Remote Sensing of Environment*, *112*, 2729–2740.

Zhu, Z., & Woodcock, C. E. (2012). Object-based cloud and cloud shadow detection in Landsat imagery. *Remote Sensing of Environment*, *118*, 83–94.